



Article

Hydrogen-Assisted Fatigue Propagation in Corner Cracks at Holes Located in Plates under Tensile Loading

Jesús Toribio * , Beatriz González and Juan-Carlos Matos 

Fracture and Structural Integrity Research Group, University of Salamanca, 37080 Salamanca, Spain; bgonzalez@usal.es (B.G.); jcmatos@usal.es (J.-C.M.)

* Correspondence: toribio@usal.es; Tel.: +34-677566723

Abstract: In this study, hydrogen-assisted fatigue propagation (a kind of corrosion fatigue phenomenon) in corner cracks at holes located in plates under tensile loading was studied, the results compared with those obtained for propagation by fatigue in air. To this end, numerical modeling was carried out for the case studied to evaluate the advance of the crack front based on the Paris equation and the stress intensity factors (SIFs) obtained by Raju and Newman. The results showed that the cracks tended toward a preferential propagation path in their growth, the effect of the presence of the stress concentrator on the preferential fatigue propagation path being more pronounced in the crack growth by fatigue in air than in the crack growth by corrosion fatigue.

Keywords: corner flaws; plates with holes; stress concentrators; numerical modeling; Paris law; fatigue crack propagation; aspect ratio; preferential propagation path.



Citation: Toribio, J.; González, B.; Matos, J.-C. Hydrogen-Assisted Fatigue Propagation in Corner Cracks at Holes Located in Plates under Tensile Loading. *Metals* **2021**, *11*, 552. <https://doi.org/10.3390/met11040552>

Academic Editors: Mauro Madia and Luis Filipe Borrego

Received: 31 January 2021
Accepted: 23 March 2021
Published: 29 March 2021

Publisher's Note: MDPI stays neutral with regard to jurisdictional claims in published maps and institutional affiliations.



Copyright: © 2021 by the authors. Licensee MDPI, Basel, Switzerland. This article is an open access article distributed under the terms and conditions of the Creative Commons Attribution (CC BY) license (<https://creativecommons.org/licenses/by/4.0/>).

1. Introduction

The study of fatigue crack propagation in plates containing stress concentrators (holes or notches) is of great interest in the field of fracture mechanics. In this framework, the stress intensity factor (SIF) has been frequently calculated (both numerically and experimentally) for cases of corner cracks (symmetrical or asymmetrical, one or two) emanating from a hole [1–8] or for single cracks (also of the corner type) emerging from a notch [9,10]. The SIF in quarter-elliptical corner cracks emanating from a notch placed in a plate under tension loading has been calculated using finite element analysis (with 3D meshes of the cracked plate and singular elements in the crack tip) together with the nodal force method [2,9] and the quarter-point displacement or J -integral methods [6,10].

The finite element method (FEM), without explicitly including the crack in the mesh, has also been used together with a simple engineering method [8], with a mathematical splitting scheme [7] and with an iterative superposition of a finite element solution for stresses in the unflawed body and an analytic solution for stresses in an infinite solid containing a flat elliptical crack [1]. Empirical SIFs obtained using photoelastic frozen stress tests [3] and digitized data on the fatigue growth [4] agree well with the SIFs calculated with the finite element method. It is possible to apply the SIF solutions for cases of two symmetric quarter-elliptical corner cracks emerging from a hole in large plates to cases where there is a single corner crack in a finite-sized plate using certain empirical correction factors [5].

Under tension, cracks in the corner of a plate have higher SIF values for the points of the front near both free surfaces (they are maximum in the proximity of one or the other depending on the crack aspect ratio) and lower ones for the inner points [11]. For corner cracks originating in the semicircular notch of a plate subjected to tension, the SIF is usually greater at the points of the crack front near the notch [9]. For a case in which a crack presented aspect ratios (crack depth-to-crack length ratio) equal to 0.2, the maximum SIF was found to occur near the intersection of the crack with the hole surface for shallow cracks and at the front surface for deep cracks [2]. For a case in which the crack

presented aspect ratios (crack depth-to-crack length ratio) equal to 2, the SIF was found to be almost constant along the entire crack front [10]. For corner-type cracks emerging from a semicircular notch or a through hole, the SIF rises (for the same crack configuration) with the increase in the ratio between the notch radius (or hole) and the thickness of the plate [6,10].

Cracks in plates, during their advance by fatigue, tend toward a preferential propagation path [12–14]. The existence of free surfaces influences the advance of the crack, so that although it tries to propagate while maintaining the SIF constant (*iso-K*) along its front, the free surface of the plate prevents it [15]. The corner cracks originating from holes located in plates are propagated by fatigue (in tension) slightly faster along the hole, maintaining an elliptical geometry during growth [16]. The crack advance tends asymptotically to a preferential pattern, so that the aspect ratio approaches a constant value, greater with the decrease in the radius of the hole and the increase in the Paris exponent of the material [17,18]. The cold expansion of the drills causes a delay in the advance of the crack due to the presence of compressive residual stresses [19].

High-strength low-alloy (HSLA) steels demonstrate high strength-to-weight ratios and good atmospheric corrosion resistance. They can be considered as microalloyed steel and are used for manufacturing structures, ships, cranes, pipes for oil and so on. In HSLA steels, fatigue crack growth in water was found to be higher than that in air due to anodic dissolution and possible H embrittlement effects, while fatigue crack growth in NaOH solution was significantly less than that in air [20]. In relation to the influence of hydrogen on fatigue, the hydrogen effect was found to increase with decreasing SIF range and with the increase in exposure time [21]. Welded joints in HSLA steels are areas of weakness [22,23]; an alternative is threaded joints, where holes have to be made. Non-load carrying spot-welded joints have a significantly lower fatigue limit compared to specimens with a drilled hole [24]. It has been observed that the large defects inherent to each hole-making procedure are those that determine the fatigue failure, regardless of the studied HSLA grades [25].

The novelty of this study was that the authors numerically examined the hydrogen-assisted fatigue propagation paths of corner cracks (with different initial geometries) at holes located in HSLA-80 steel plates under tensile cyclic loading, comparing the results with those obtained for fatigue in air. In addition, the effects of the environment and the hole size on the fatigue preferential propagation path were analyzed.

2. Numerical Procedure

The material used in this study was a Cu-strengthened HSLA-80 steel. Roy, Manna and Chattoraj [21] studied the fatigue crack growth for this steel during hydrogen charging, finding that the increase in the charging current density raises the Paris constant C and decreases the slope m . Thus, the value of the Paris exponent was $m = 3.2$ in air-tested specimens and $m = 0.6$ in the sample after hydrogen charging at 1 mA/cm^2 . The steel had a yield strength of 650 MPa and an ultimate tensile strength of 740 MPa.

Numerical modeling was performed in Java language to study the advance paths of corner-type cracks located on plates of great length, high width w and finite thickness t , subjected to cyclic tensile loading. The cracks emerge from a corner of the plate (Figure 1a) or from the edge of a hole of radius r (Figure 1b), propagating through the cross-section of the plate.

The crack front was modeled as a quarter-ellipse of semiaxes a (crack depth) and b (crack length). Each point p on the crack front was characterized by the angular parameter ϕ , which depends on the ratio between the semiaxes a and b of the ellipse (Figure 2).

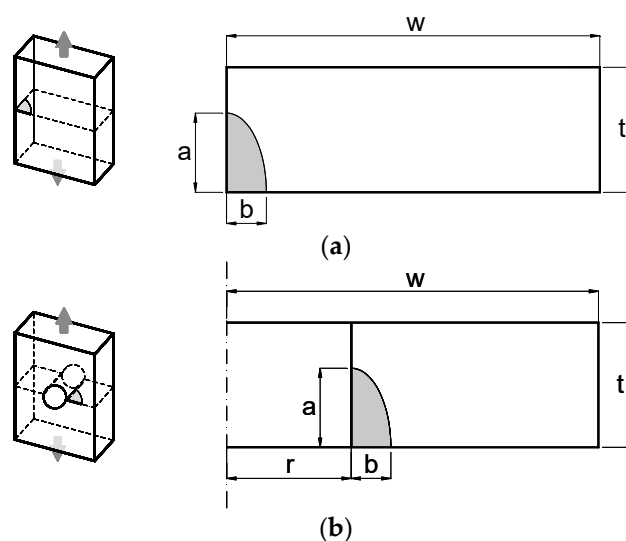


Figure 1. Crack emanating from: (a) the corner of a plate; (b) a hole.

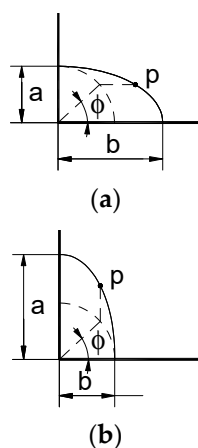


Figure 2. Angle ϕ defining a point p of the crack front: (a) $a/b \leq 1$; (b) $a/b > 1$.

The SIFs K used in this study were those obtained by Raju and Newman [2,11,26] by means of a 3D finite element analysis and the nodal force method. For a plate subjected to remote tension σ , with a crack of quarter-ellipse geometry emerging from a corner (Figure 1a), these authors [2,26] fitted the results to the equation:

$$K = \sigma \sqrt{\frac{\pi a}{Q}} F_1 \quad (1)$$

The function Q is the form factor for an ellipse (which is given by the square of the complete elliptic integral of the second class) depending on the crack aspect ratio a/b . The function F_1 depends on the parameters: crack aspect ratio a/b , relative crack depth a/t , finite width b/w and angular location ϕ . This function is valid for $0.2 \leq a/b \leq 2$, $a/t < 1$, $b/w < 0.5$ and $0 \leq \phi \leq \pi/2$ [2,26].

For a plate subjected to remote stress with a quarter-ellipse corner-type crack emanating from a through hole (Figure 1b), Raju and Newman [11,26] obtained the equation:

$$K = \sigma \sqrt{\frac{\pi a}{Q}} F_2 \quad (2)$$

The function F_2 depends on the same parameters as F_1 and, in addition, it also depends on the radius–thickness ratio r/t and radius–width ratio r/w . This function is valid for $0.2 \leq a/b \leq 2$, $a/t < 1$, $0.5 \leq r/t \leq 2$, $(r + b)/w < 0.5$ and $0 \leq \phi \leq \pi/2$ [11,26].

The basic hypothesis of this modeling consists of assuming that each point at the crack front propagates by fatigue in the direction perpendicular to such a front, according to the Paris–Erdogan law [27]

$$\frac{da}{dN} = C\Delta K^m \quad (3)$$

by maintaining the elliptical geometry throughout the calculation process, as has been shown in experimental [13] and numerical [14] ways.

The crack front was discretized in a set of points, by dividing them into z segments of identical length using the Simpson rule. Next, each point i was shifted in a perpendicular manner to the crack front according to the Paris–Erdogan law [27]. At point i of maximum SIF $F\{\max\}$ the maximum crack increase $\Delta a\{\max\} \equiv \max \Delta a(i)$ (of constant value throughout the full calculation) was applied, while for the other points the advance $\Delta a(i)$ was calculated through the equation:

$$\Delta a(i) = \Delta a\{\max\} \left[\frac{F(i)}{F\{\max\}} \right]^m \quad (4)$$

Finally, the calculated points were fixed to a quarter-ellipse geometry (using the least squares method), thereby obtaining another crack front that allowed the process to be started again (it can be repeated iteratively until the desired depth is achieved).

A convergence study was carried out to determine the value of the parameters z and $\Delta a\{\max\}$. The propagation of cracks with relative crack depths in the range $0 < a/t < 0.1$ is not shown in the results, because convergence problems occurred.

3. Numerical Results

Figures 3–8 show the advance of corner-type cracks (with several initial geometries: relative crack depth $(a/t)_0 = \{0.1, 0.2, 0.3, 0.4, 0.5, 0.6, 0.7\}$ and crack aspect ratio $(a/b)_0 = \{2, 1, 0.2\}$) located in plates subjected to air fatigue ($m = 3.2$) or corrosion fatigue in a hydrogen environment ($m = 0.6$) under tensile loads. Figures 3 and 6 correspond to the results for a crack located in the corner of a plate, Figures 4 and 7 with those of a corner type originating in a hole of radius $r/t = 2$ and Figures 5 and 8 with those of a corner type emanating from a hole of smaller radius than in the previous case, $r/t = 0.5$.

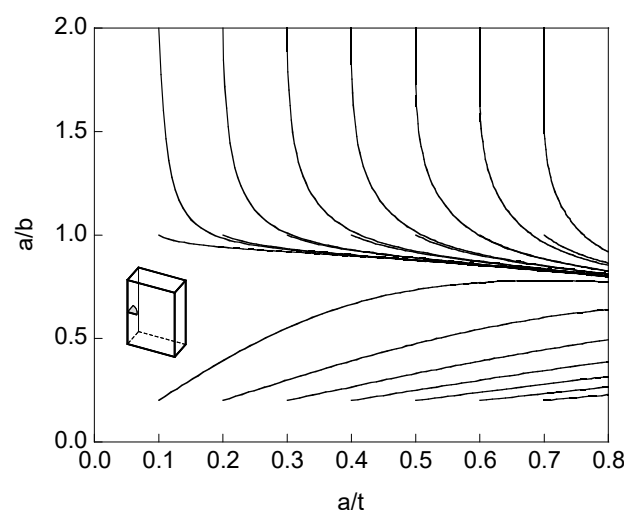


Figure 3. Crack aspect ratio evolution during fatigue propagation in air for cracks emanating from a plate corner.

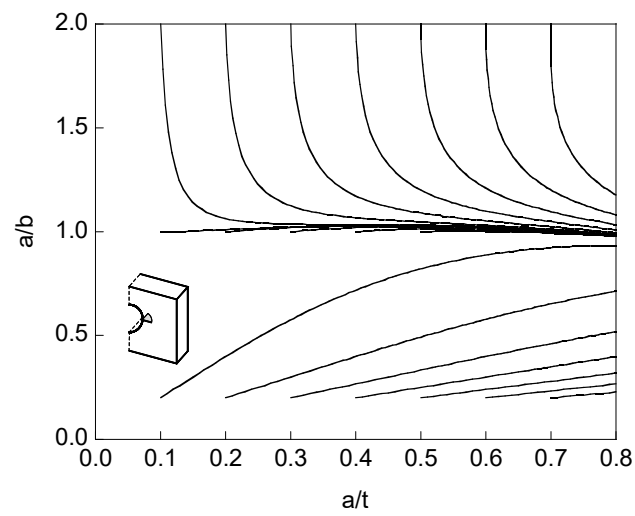


Figure 4. Crack aspect ratio evolution during fatigue propagation in air for cracks emanating from a hole with $r = 2t$.

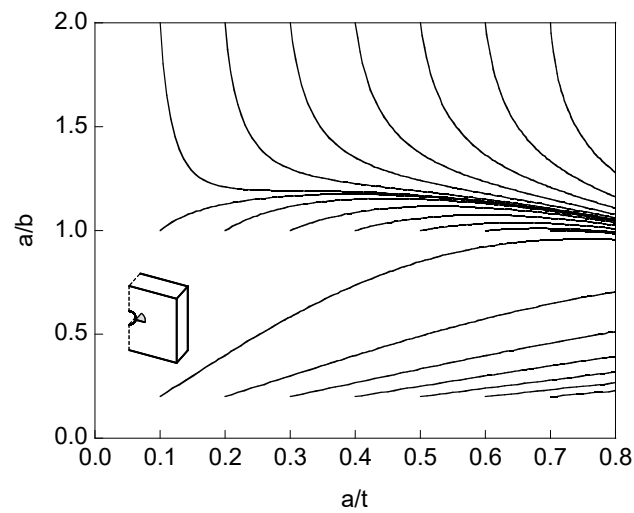


Figure 5. Crack aspect ratio evolution during fatigue propagation in air for cracks emanating from a hole with $r = 0.5t$.

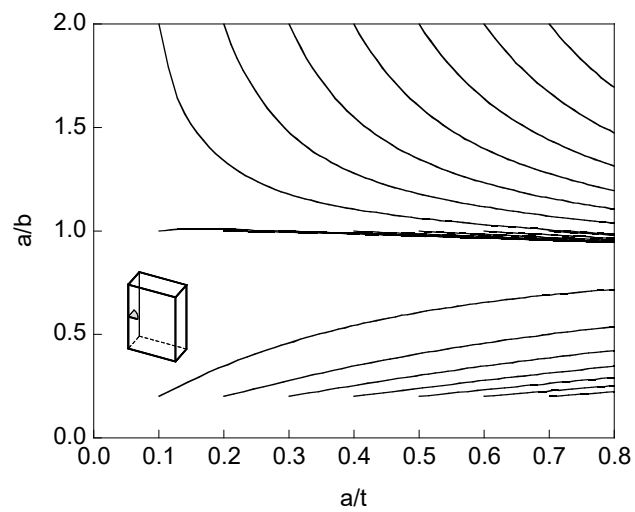


Figure 6. Crack aspect ratio evolution during corrosion fatigue propagation for cracks emanating from a plate corner.

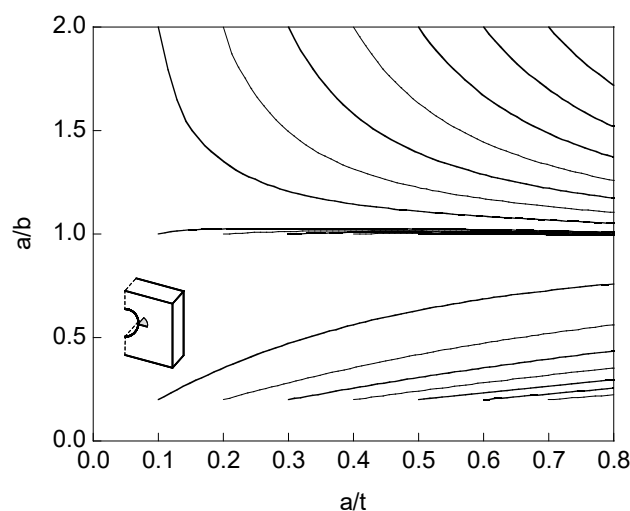


Figure 7. Crack aspect ratio evolution during corrosion fatigue propagation for cracks emanating from a hole with $r = 2t$.

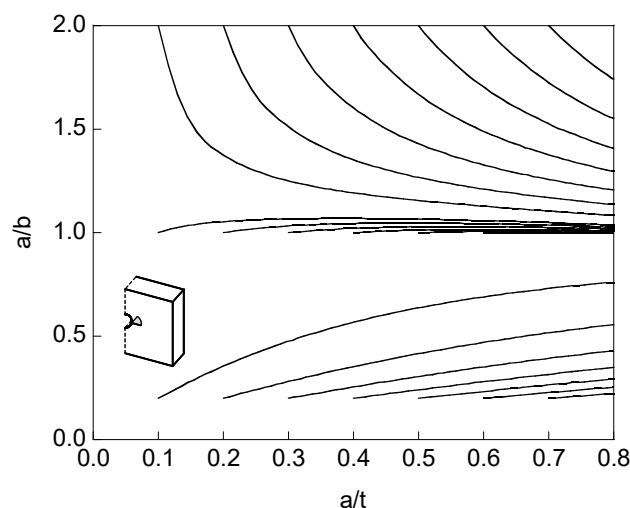


Figure 8. Crack aspect ratio evolution during corrosion fatigue propagation for cracks emanating from a hole with $r = 0.5t$.

The propagation paths for a single corner-type crack emanating from a hole (Figures 4, 5, 7 and 8) are the same as in the case of two symmetrical corner cracks strating in a hole, since the relation between the SIFs in both cases, for each point of the crack front (in the same crack geometry), is the same [2,26] and does not affect the calculation.

The fatigue crack growth from different initial geometries tends towards a preferential propagation path, which approximately corresponds to that of a very shallow initial crack of quasi-circular front $a/b \sim 1$, with a faster convergence (approach between the different propagation curves $a/b-a/t$) for cracks originating in the corner of a plate than for those emanating from a hole. For this latter case, the convergence is greater when the ratio between the radius of the hole and the thickness of the plate r/t is increased.

The proximity between the propagation curves $a/b-a/t$ is greater in air fatigue than in corrosion fatigue. Such a proximity increases through the reduction of the initial relative crack depth $(a/t)_0$ and the increase of the closeness between the initial crack geometry $((a/t)_0, (a/b)_0)$ and the preferential propagation path. Thus, cracks with an elevated initial aspect ratio $((a/b)_0 = \{1, 2\})$ (upper part of the plots) present a greater convergence than those of initial quasi-straight geometry $((a/b)_0 = 0.2)$ (lower part of the plots), which, for elevated initial relative depths (lower right-hand part of the plots), are quasi-straight $a/b-a/t$ paths, really similar for all studied cases.

4. Discussion

Figure 9 shows the crack aspect ratio *vs.* relative crack depth curves corresponding to the preferential propagation path $(a/b - a/t)_P$ for the configurations studied (fatigue in air, $m = 3.2$, and corrosion fatigue, $m = 0.6$; crack emanating from a corner and from a hole of radius $r/t = \{0.5, 2\}$).

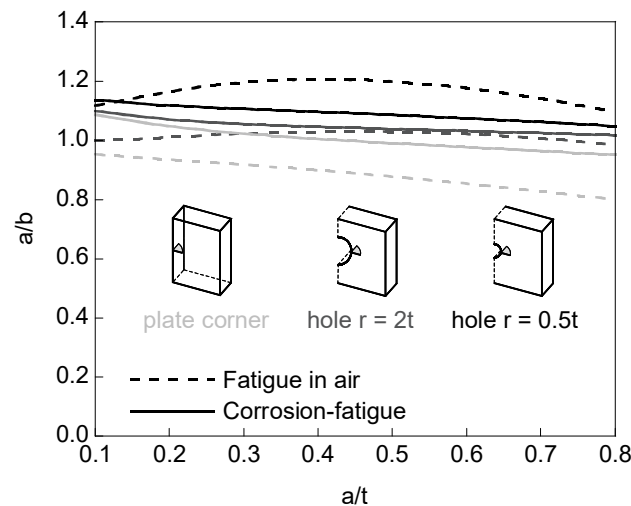


Figure 9. Preferential propagation paths.

In corrosion fatigue and fatigue in air, the preferential propagation path curves $(a/b - a/t)_P$ show a higher aspect ratio a/b for the same crack relative depth a/t when a hole is present in the plate, the value increasing more by decreasing the hole radius. In addition, for corrosion fatigue ($m = 0.6$) the three curves (plate without a hole and plate with a hole of radius $r/t = \{0.5, 2\}$) are closer to each other than in the case of fatigue in air ($m = 3.2$), such that the effect of the presence of the stress concentrator on the preferential propagation path is more pronounced in the crack propagation by fatigue in air than in the crack propagation by corrosion fatigue.

In the curve of the preferential propagation path corresponding to the crack advance by air fatigue in a plate without a hole, it can be observed that the crack aspect ratio always decreases with the crack relative depth, whereas, if the plate presents a hole, the crack aspect ratio first increases with the crack relative depth and then decreases, this effect being more pronounced as the hole radius decreases. In contrast, in the corrosion fatigue for the three cases studied (plates without hole and with hole of radius $r/t = \{0.5, 2\}$), the preferential propagation paths show that the crack aspect ratio always decreases with the crack relative depth.

Figures 10–15 present the evolution of the dimensionless SIF $K/\sigma(\pi a)^{1/2}$ along the crack front for the cracks linked to the preferential propagation path with depths $a/t = \{0.1, 0.2, 0.3, 0.4, 0.5, 0.6, 0.7, 0.8\}$. The free surfaces raise the SIF in the crack-front points near to them, presenting smaller values for the inner zones. In addition, in cracks originated from holes, the SIF is greater in the region of the crack front close to the hole (Figures 11, 12, 14 and 15). The decrease in the radius of the hole produces a greater gradient of the SIF, but also decreases its area of influence. For short cracks there is a greater variation in the SIF because the majority of the crack front is in the region of influence of the stress concentrator. However, when the crack is deeper, part of the front is in a region of lower stress gradient.

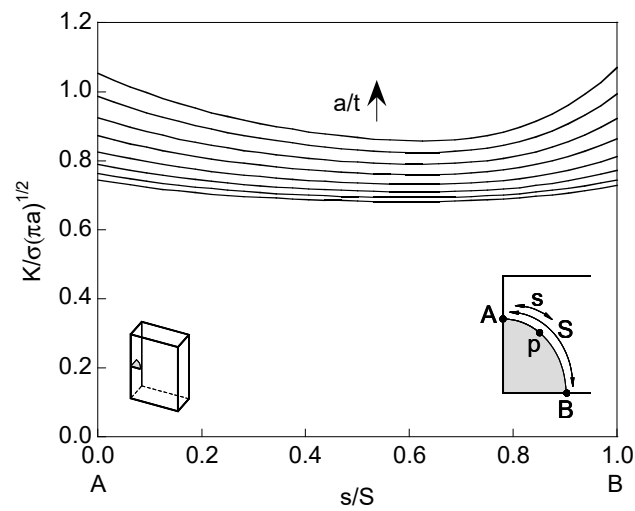


Figure 10. Dimensionless stress intensity factor (SIF) along the crack front for the preferential fatigue propagation path (fatigue in air; cracks emanating from a plate corner).

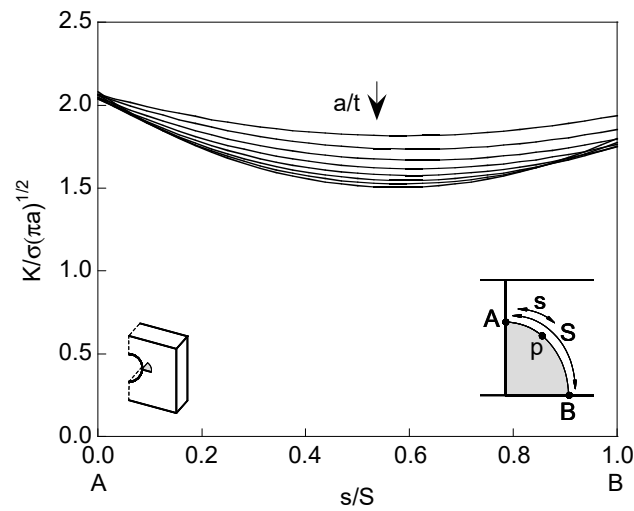


Figure 11. Dimensionless SIF along the crack front for the preferential fatigue propagation path (fatigue in air; cracks emanating from a hole with $r = 2t$).

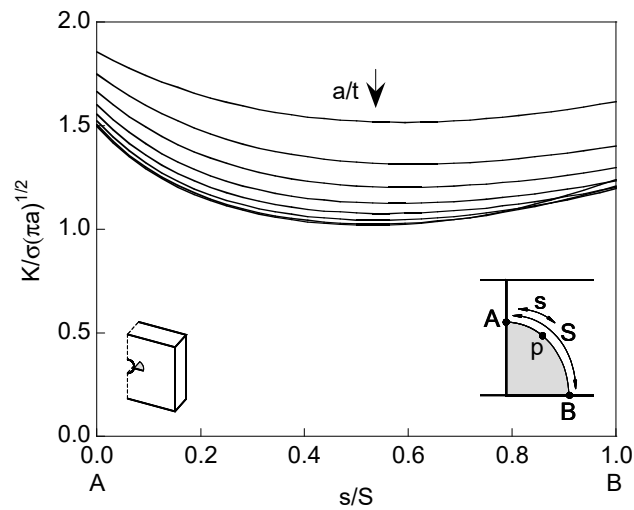


Figure 12. Dimensionless SIF along the crack front for the preferential fatigue propagation path (fatigue in air; cracks emanating from a hole with $r = 0.5t$).

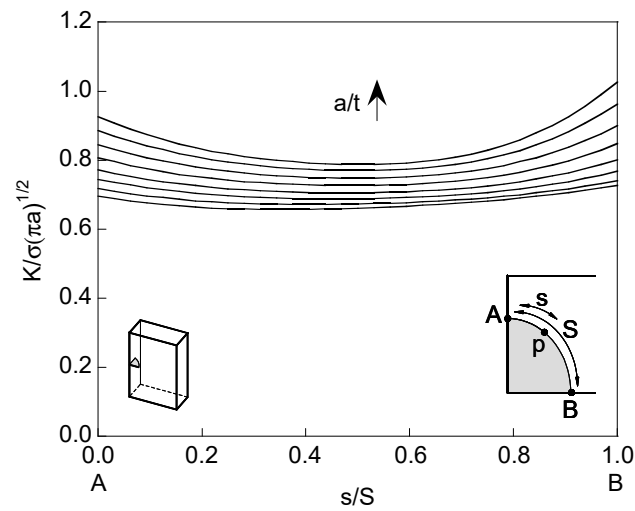


Figure 13. Dimensionless SIF along the crack front for the preferential fatigue propagation path (corrosion fatigue; cracks emanating from a plate corner).

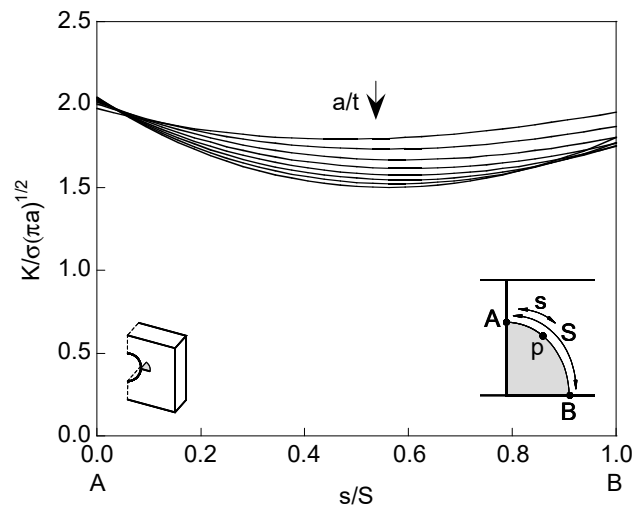


Figure 14. Dimensionless SIF along the crack front for the preferential fatigue propagation path (corrosion fatigue; cracks emanating from a hole with $r = 2t$).

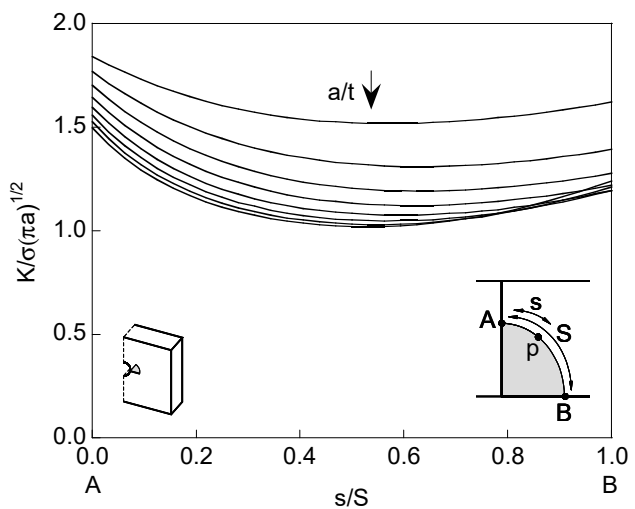


Figure 15. Dimensionless SIF along the crack front for the preferential fatigue propagation path (corrosion fatigue; cracks emanating from a hole with $r = 0.5t$).

The curves corresponding to the preferential propagation paths in fatigue can be fitted to fourth degree polynomial equations (with correlation coefficients < 0.0004):

$$\left(\frac{a}{b}\right)_P = A + B\left(\frac{a}{t}\right)_P + C\left(\frac{a}{t}\right)_P^2 + D\left(\frac{a}{t}\right)_P^3 + E\left(\frac{a}{t}\right)_P^4 \quad (5)$$

for which the values of the coefficients A , B , C , D and E for the different cases studied are shown in the Table 1.

Table 1. Coefficients for Equation (5).

Environment	r/t	A	B	C	D	E
Air	–	1.14226	–0.663195	1.19311	–1.15887	0.412712
	2	1.14307	–0.546965	1.16221	–1.18695	0.426212
	0.5	1.16205	–0.314444	0.623563	–0.741959	0.287784
Hydrogen	–	0.970317	–0.187459	0.124991	–0.321309	0.155703
	2	0.990338	0.0352184	0.546897	–1.21531	0.583372
	0.5	1.02962	0.981150	–1.67329	0.914044	–0.283772

5. Conclusions

Corner cracks at holes located in plates subject to cyclic tensile loading, with different initial geometries, approximate during their fatigue growth towards a *preferential propagation path* $(a/b-a/t)_P$, different in fatigue in air than in corrosion fatigue.

The convergence, closeness rate between the crack growth curves $a/b-a/t$ from distinct initial geometries, was quicker for fatigue in air (greater exponent m of Paris) than for corrosion fatigue and when the hole relative radius r/t was increased (still greater if there is no hole).

Crack advance according to the preferential propagation path showed a greater crack aspect ratio a/b , for the same crack relative depth a/t , when there was a hole than when there was no hole, increasing its value when the hole relative radius r/t decreased.

In corrosion fatigue the preferential propagation path curves $(a/b-a/t)_P$ were closer to each other than in the case of fatigue in air, so that the effect of the presence of the stress concentrator on the preferential propagation path was more pronounced in fatigue in air than in corrosion fatigue.

Future research directions in which the obtained models could be practically applied would involve hydrogen-assisted fatigue propagation effects in corner cracks at holes located in plates under tensile loading. In practical terms, these models could be applied to the analysis of fractures of HSLA-80 steels subjected to fatigue loading.

Author Contributions: J.T., J.-C.M. and B.G. conceived and designed the numerical modeling; J.-C.M. developed the computer programs; J.T., J.-C.M. and B.G. analyzed the data; J.T. and B.G. wrote the paper. All authors have read and agreed to the published version of the manuscript.

Funding: This research was funded by the following Spanish institutions: Ministry for Science and Technology (MICYT; Grant MAT2002-01831), Ministry for Education and Science (MEC; Grant BIA2005-08965), Ministry for Science and Innovation (MICINN; Grant BIA2008-06810), Ministry for Economy and Competitiveness (MINECO; Grant BIA2011-27870), Junta de Castilla y León (JCyL; Grants SA067A05, SA111A07, SA039A08 and SA132G18).

Institutional Review Board Statement: Not applicable.

Informed Consent Statement: Not applicable.

Data Availability Statement: Not applicable.

Conflicts of Interest: The authors declare no conflict of interest. The funders had no role in the design of the study; in the collection, analyses, or interpretation of data; in the writing of the manuscript, and in the decision to publish the results.

List of Symbols

a	Crack depth
a/b	Crack aspect ratio
$(a/b)_0$	Initial crack aspect ratio
$(a/b)_P$	Crack aspect ratio for preferential propagation path
a/t	Relative crack depth
$(a/t)_0$	Initial relative crack depth
$(a/t)_P$	Relative crack depth for preferential propagation path
A	Crack-front point corresponding to the crack depth
$\Delta a(i)$	Crack advance at the point i
$\Delta a\{\max\}$	Maximum crack advance in the iterations
b	Crack length
B	Crack front-point corresponding to the crack length
C	Paris constant
da/dN	Crack growth rate
F_1	Parameter to obtain the SIF in a corner crack
F_2	Parameter to obtain the SIF in a corner crack at a hole
$F(i)$	Parameter F at the point i
$F\{\max\}$	Maximum parameters F along the crack front
ϕ	Angle characterizing a point at the crack front
i	Crack front discrete point
K	Stress intensity factor (SIF)
ΔK	Stress intensity factor range
m	Paris exponent
Q	Parameter to obtain K
r	Hole radius
r/t	Relative hole radius
s	Ellipse arc length characterizing a crack front-point
S	Quarter-ellipse length characterizing crack front
σ	Remote tension
t	Plate thickness
w	Plate width

List of Abbreviations

FEM	Finite element method
HSLA	High-strength low-alloy
SIF	Stress intensity factor

References

1. Kullgren, T.E.; Smith, F.W.; Ganong, G.P. Quarter elliptical cracks emanating from hole in plates. *Trans. ASME* **1978**, *100*, 144–149. [[CrossRef](#)]
2. Raju, I.S.; Newman, J.C., Jr. Stress-intensity factors for two symmetric corner cracks. In *Fracture Mechanics*; Smith, C.W., Ed.; American Society for Testing and Materials: West Conshohocken, PA, USA, 1979; pp. 411–430.
3. Nicoletto, G. Stress-intensity distributions for corner cracks emanating from open holes in plates of finite width. *Theor. Appl. Fract. Mech.* **1985**, *3*, 63–70. [[CrossRef](#)]
4. Schijve, J. Comparison between empirical and calculated stress intensity factors of hole edge cracks. *Eng. Fract. Mech.* **1985**, *22*, 49–58. [[CrossRef](#)]
5. Shin, C.S. The stress intensity of corner cracks emanating from holes. *Eng. Fract. Mech.* **1990**, *37*, 423–436. [[CrossRef](#)]
6. Lin, X.B.; Smith, R.A. Stress intensity factors for corner cracks emanating from fastener holes under tension. *Eng. Fract. Mech.* **1999**, *62*, 535–553. [[CrossRef](#)]
7. Fawaz, S.A.; Andersson, B. Accurate stress intensity factor solutions for corner cracks at a hole. *Eng. Fract. Mech.* **2004**, *71*, 1235–1254. [[CrossRef](#)]
8. Peng, D.; Wallbrink, C.; Jones, R. Stress intensity factor solutions for finite body with quarter-elliptical flaws emanating from a notch. *Eng. Fract. Mech.* **2005**, *72*, 1329–1343. [[CrossRef](#)]

9. Tan, P.W.; Newman, J.C., Jr.; Bigelow, C.A. Three-dimensional finite-element analyses of corner cracks at stress concentrations. *Eng. Fract. Mech.* **1996**, *55*, 505–512. [[CrossRef](#)]
10. Shivakumar, K.N.; Newman, J.C., Jr. Stress intensity factors for large aspect ratio surface and corner cracks at a semi-circular notch in a tension specimen. *Eng. Fract. Mech.* **1991**, *38*, 467–473. [[CrossRef](#)]
11. Raju, I.S.; Newman, J.C., Jr. *Finite-Element Analysis of Corner Cracks in Rectangular Bars (NASA Technical Memorandum 89070)*; NASA: Hampton, VA, USA, 1987.
12. Toribio, J.; Matos, J.C.; González, B. Aspect ratio evolution associated with surface cracks in sheets subjected to fatigue. *Int. J. Fatigue* **2016**, *92*, 588–595. [[CrossRef](#)]
13. Toribio, J.; Matos, J.C.; González, B. Corrosion-fatigue crack growth in plates: A model based on the Paris law. *Materials* **2017**, *10*, 439. [[CrossRef](#)]
14. Toribio, J.; Matos, J.C.; González, B. Aspect ratio evolution in embedded, surface, and corner cracks in finite-thickness plates under tensile fatigue loading. *Appl. Sci.* **2017**, *7*, 746. [[CrossRef](#)]
15. Lin, X.B.; Smith, R.A. Finite element modelling of fatigue crack growth of surface cracked plates. Part III: Stress intensity factor and fatigue crack growth life. *Eng. Fract. Mech.* **1999**, *63*, 541–556. [[CrossRef](#)]
16. Grandt, A.F., Jr.; Macha, D.E. Digitized measurements of the shape of corner cracks at fastener holes. *Eng. Fract. Mech.* **1983**, *17*, 63–73. [[CrossRef](#)]
17. Lin, X.B.; Smith, R.A. Fatigue shape analysis for corner cracks at fastener holes. *Eng. Fract. Mech.* **1998**, *59*, 73–87. [[CrossRef](#)]
18. Liu, C.; Chu, S. Prediction of shape change of corner crack by fatigue crack growth circles. *Int. J. Fatigue* **2015**, *75*, 80–88. [[CrossRef](#)]
19. Lacarac, V.; Smith, D.J.; Pavier, M.J.; Priest, M. Fatigue crack growth from plain and cold expanded holes in aluminium alloys. *Int. J. Fatigue* **2000**, *22*, 189–203. [[CrossRef](#)]
20. Roy, A.; Tarafder, S.; Sivaprasad, S.; Das, S.K.; Manna, I.; Chattoraj, I. Fatigue crack growth retardation in an HSLA steel in benign environments. *Int. J. Fatigue* **2007**, *29*, 254–260. [[CrossRef](#)]
21. Roy, A.; Manna, I.; Chattoraj, I. Anomalies in hydrogen enhanced fatigue of a high strength steel. *Int. J. Fatigue* **2014**, *59*, 14–22. [[CrossRef](#)]
22. Miletić, I.; Ilić, A.; Nikolić, R.R.; Ulewicz, R.; Ivanović, L.; Szczygiol, N. Analysis of selected properties of welded joints of the HSLA steels. *Materials* **2020**, *13*, 1301. [[CrossRef](#)]
23. Ślęzak, T. Fatigue examination of HSLA steel with yield strength of 960 MPa and its welded joints under strain mode. *Metals* **2020**, *10*, 228. [[CrossRef](#)]
24. Hamel, F.G.; Masounave, J. The fatigue behavior of HSLA non-load carrying spot welded joints. *Can. Metall. Q.* **1990**, *29*, 313–318. [[CrossRef](#)]
25. Jiménez-Peña, C.; Goulas, C.; Preußner, J.; Debruyne, D. Failure mechanisms of mechanically and thermally produced holes in high-strength low-alloy steel plates subjected to fatigue loading. *Metals* **2020**, *10*, 318. [[CrossRef](#)]
26. Newman, J.C., Jr.; Raju, I.S. Stress-intensity factor equations for cracks in three-dimensional finite bodies subjected to tension and bending loads. In *Computational Methods in the Mechanics of Fracture*; Atluri, S.N., Ed.; Elsevier Science Publishers: Amsterdam, The Netherlands, 1986; Volume 2, pp. 311–334.
27. Paris, P.C.; Erdogan, F. A critical analysis of crack propagation laws. *J. Basic Eng.* **1963**, *85*, 528–534. [[CrossRef](#)]